doi.org/10.1002/batt.202000293

Electrochemical Performance of Mg Metal-Quinone Battery in Chloride-Free Electrolyte

Tjaša Pavčnik,[a, b] Jan Bitenc,*[a] Klemen Pirnat,[a] and Robert Dominko[a, b, c]

Mg batteries are a promising energy storage system due to the high capacity of the Mg metal anode. However, until recently Mg battery practical application seemed very distant due to corrosive nature of Mg electrolytes and the lack of suitable cathode materials. In this work, we bridge this gap by combining novel chloride-free Mg electrolyte, Mg perfluorinated pinacolato borate (MgFPB), with quinone based organic cathode. ATR-IR spectroscopy and complementary energy dispersive X-ray spectroscopy (EDS) of *ex situ* cathodes confirm reduction of carbonyl group during discharge an its preferred coordination with Mg^{2+} cations, although monovalent not fully dissociated $MgFPB^{+}$ cation pairs are detected as well. Mediocre capacity retention of PAQS/CNTs is improved through the use of phenanthrenequinone based polymer (PFQ/rGO). The study demonstrates the promising performance of organic compounds in chloride-free electrolytes and points towards future steps on the path towards practical Mg metal organic batteries.

1. Introduction

A key for wider market penetration of electrochemical energy storage is the development of cost-effective battery technologies. Among them, Li-ion batteries (LIBs) are currently the most mature technology and are dominating the market due to the high energy density and long cycle life. Their use is still handicapped by safety concerns and a relatively high cost, since Li, Co and natural graphite are neither very abundant nor geographically evenly distributed.[1] Therefore, researchers are actively pursuing alternative battery technologies that would offer comparable or higher energy densities and would be based on cheap sustainable materials with a low CO_2 footprint. Several different alternative battery technologies have been researched in the last decades (Li–S, Na-ion, multivalent batteries). One of the highly prospective battery systems are Mg metal batteries. Mg metal possesses a high volumetric capacity (3843 mAh cm^{-3}), almost twice as high as Li metal (2063 mAh cm^{-3}) and more than four times higher than graphite anode (837 mAh cm^{-3}). Mg metal is less prone to dendrite formation,[2,3] which makes practical Mg metal anode batteries much more realistic than Li metal ones. Although, it has to be noted that some studies report uneven Mg deposition in the laboratory cells,[4,5] which could be detrimental to cell operation with metallic Mg without any protective layer.

The practical development of Mg batteries has been hindered by the lack of Mg electrolytes stable with Mg metal anode and suitable cathode materials. Aprotic polar solvents, such as carbonates, which are widely used in LIBs, are unsuitable for Mg electrolytes,[6] as they are readily reduced on the Mg anode, forming a passive layer. Although this is also true for Li-metal/electrolyte interface, the solid-electrolyte interface (SEI) formed on the Li-metal electrode is permeable to Li^{+} ions, whereas the passive layer formed on Mg-metal electrode is a poor conductor of Mg^{2+} ions.[7] Thus, most studies focus on the use of ether-functional solvents, especially glymes and tetrahydrofuran, which are compatible with metallic Mg and can stabilize Mg^{2+} ions via coordination through the electron-donating ether oxygen atoms, but suffer from lower oxidative stability.[7] However, it was recently shown that even dimethoxyethane (DME) can be reduced on the Mg interface.[6] The use of ethereal solvents and the requirement of reductive stability on Mg metal tremendously limit the number of viable salts that can be used for Mg-based electrolytes. Additionally, Mg^{2+} ion possesses much higher charge density due to the divalent nature at approximately the same ion radius of the ion as Li^{+}. Increased charged density increases the strength of interactions with both solvents and cathode host material as well as decreases mobility of Mg^{2+} inside cathode structures. Despite very attractive properties of Mg anode, searching for appropriate electrolyte and cathode material for the Mg system remains up to date a considerable challenge.

Reversible deposition of Mg from the solution was first discovered in the early 1920th using Grignard reagents.[8] In the next decades, different Mg reagents that enable Mg deposition from the solution were investigated, most of them were based on Mg–Cl complexes.[9–16] A big drawback of chloride-containing electrolytes is the corrosive nature of Cl^{-}, which leads to

[a] T. Pavčnik, Dr. J. Bitenc, Dr. K. Pirnat, Prof. Dr. R. Dominko
Department of Materials Chemistry
National Institute of Chemistry
Hajdrihova 19, 1000 Ljubljana, Slovenia
E-mail: jan.bitenc@ki.si
[b] T. Pavčnik, Prof. Dr. R. Dominko
Faculty of Chemistry and Chemical Technology
University of Ljubljana
Večna pot 113, 1000 Ljubljana, Slovenia
[c] Prof. Dr. R. Dominko
Alistore-European Research Institute
CNRS FR 3104, Hub de l'Energie
Rue Baudelocque 80039 Amiens, France

Supporting information for this article is available on the WWW under https://doi.org/10.1002/batt.202000293

incompatibility with non-noble current collectors such as stainless steel and aluminum,[16] presenting an insurmountable challenge for production. Furthermore, some of the active species, formed in the solution are nucleophilic in their nature and cannot be used with electrophilic cathode materials (sulfur, organic materials). Therefore, there is a strong incentive for the development of non-corrosive and non-nucleophilic electrolytes for Mg batteries.

A few chloride-free magnesium salts that have been reported so far are shown in Table 1. The main issue of the first developed electrolytes was their low oxidative stability, together with modest Coulombic efficiency of Mg stripping/deposition. Better stability has been reached with the synthesis of Mg carborane salt, however, the synthesis of carborane is quite complex and expensive, which makes practical application of carborane salts questionable.[18] To meet this challenge, Arnold *et al.*[21] demonstrated a new class of Mg salts with weakly coordinating anions. Mg fluoroalkoxyaluminates were synthesized from magnesium and aluminum fluoroalkoxides in ethereal solvents resulting in solutions that can reversibly deposit magnesium metal with near unit efficiency. Considering the fact that alkyloxyborate anions are generally less water-sensitive compared to alkyloxyaluminate anions, Fichtner *et al.*[19] developed a series of Mg salts with boron-based weakly

Table 1. Review of Cl-free salts for Mg electrolytes.

Mg salt	Structure of an anion	Electrolyte	Oxidative stability	Coulombic efficiency	Ref.
$Mg(BBu_2Ph_2)_2$	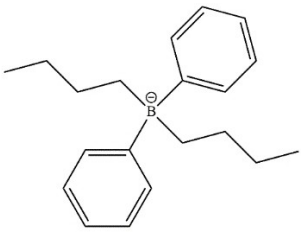	0.25 M/THF	< 2.0 V	not available	[11]
$Mg(BH_4)_2$	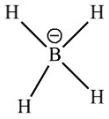	0.1 M/DME	2.0 V	67%	[17]
$Mg(BH_4)_2/LiBH_4$		0.2 M/DME	2.0 V	94%	
$Mg(TFSI)_2$	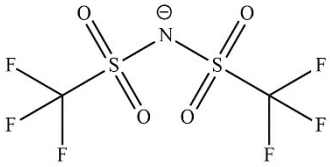	0.5 M/DME	2.3 V	70%	[22]
$Mg(CB_{11}H_{12})_2$	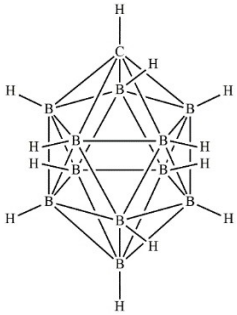	0.75 M/G4	3.8 V	94%	[18]
$Mg[X(OR^F)_4]_2$ X = Al, B	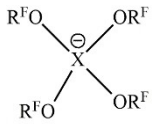	X = Al			
		OR^F = hfip,[a] 0.25 M/DME	4.0 V	99%	[18]
		OR^F = pftb,[b] 0.1 M/G3	> 4.0 V	90%	[23]
		X = B			
		OR^F = hfip,[a] 0.5 M/DME	4.0 V	98%	[19]
$Mg(FPB)_2$	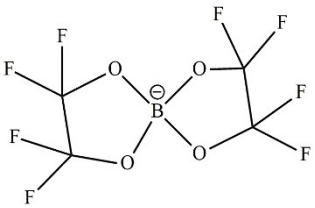	0.5 M/DGM	4.0 V	95%	[20]

[a] hfip = 1,1,1,3,3,3-hexafluoropropanol. [b] pftb = perfluoro-tert-butanol.

coordinated anions. The salts were prepared through the reaction between $Mg(BH_4)_2$ and different fluorinated alcohols. The best performance was demonstrated by $[Mg(dme)_3][B(hfip)_4]_2$ (denoted as MgBhfip, hfip = 1,1,1,3,3,3-hexafluoro-2-propanol). Further improvement was achieved through use of magnesium perfluorinated pinacolatoborate ($[Mg(dme)_3][B(O_2C_2(CF_3)_4)_2]_2$ or MgFPB).[20] Due to the chelating effect, the anion is highly stable and forms weak interactions with Mg^{2+}, which contributes to good ionic conductivity and improved electrochemical performance over MgBhfip.

Several inorganic as well as organic materials have been so far examined. Aurbach *et al.* demonstrated that Mg^{2+} ions can reversibly intercalate into the Chevrel phase (Mo_6S_8).[12] Although Mo_6S_8 showed long-term cycling stability, energy density is low. Some other inorganic materials were proposed as well, for example Ti_2S_4,[22] V_2O_5,[23] MnO_2[24] but none of them has so far shown commercial potential. On the other hand, redox active organic materials are promising in terms of both high capacity and reversibility.[25] Their weak point is fast capacity fading due to the solubility of active materials in electrolyte solutions, which can be mitigated by the polymerization of electroactive groups. Anthraquinone based polymer showed excellent rate capability and fair electrochemical stability in chloride based Mg electrolytes.[26] However, due to the corrosiveness of chloride-containing electrolytes, the practical application of such system still seems distant. Additional issue of chloride-containing electrolytes solutions is that $MgCl^+$ can act as an active charge carrier instead of Mg^{2+}. The involvement of $MgCl^+$ could hamper operation in lean electrolyte conditions and significantly reduce the practical energy density of the cell.[27]

In this work we aim to bridge the gap between the organic materials and novel, chloride-free Mg electrolytes. MgFPB and MgBhfip salts are synthesized and their performance evaluated in two most routinely used ethereal solvents. Electrolyte performance is optimized through the use of additives and combined with two different organic polymer cathodes in Mg metal–organic battery. The electrochemical mechanism of poly (anthraquinonyl sulfide) (PAQS) organic cathode in the non-nucleophilic chloride-free electrolyte is thoroughly investigated from the mechanistic point of view. Mechanism of organic polymer reaction is confirmed through use of ATR-IR spectroscopy of *ex situ* cathodes and complementary EDS analysis, which gives insight into Mg cation speciation in the discharged state.

Experimental Section

Electrolyte synthesis and characterization

MgFPB salt was synthesized according to the published procedure.[20] Briefly, $Mg(BH_4)_2$ powder was dissolved into DME (125 mM) in a two neck flask. The flask was equipped with a condenser. 4.2 equivalents of perfluorinated pinacol (PFP) were dissolved into DME (2 M) and dropwise added over a period of 0.5 h into the stirred solution of $Mg(BH_4)_2$. The reaction mixture was stirred at 60 °C for 20 h. Reaction solution was concentrated under vacuum and dry hexane was added to precipitate the MgFPB salt. After filtration, washing with dry hexane and vacuum-drying, the final product was obtained as a white microcrystalline powder (96% yield). MgBhfip salt was synthesized according to the literature procedure.[19] Prepared salts were characterized using ATR-IR and NMR spectroscopy (Figure S1–4). Electrolytes were prepared by adding the appropriate amount of the MgFPB/MgBhfip and *n*-Bu_2Mg salts into measuring flasks and diluting them up to the mark to obtain 0.4 M Mg salt/40 mM *n*-Bu_2Mg in the DME or bis(2-methoxyethyl) ether (DGM) solvents. Solvents were dried with 4 Å molecular sieves for 3 days, refluxed for one day with K/Na alloy (3/1 wt.) and then distilled. The amount of water in solvents was determined with Karl Fischer titration (< 5 ppm).

Materials preparation

PAQS, PAQS with 10% of multi-walled carbon nanotubes (PAQS/CNTs) and PFQ nanostructurized with 21 wt.% reduced graphene oxide (PFQ/rGO) were synthesized according to the procedure described in our previous publications.[28,29]

Electrochemical characterization

Electrochemical characterization of the electrolyte was performed through the galvanostatic deposition with 1 mA cm^{-2} current density on the Pt working electrode for 60 min and stripping until the cut-off voltage of 3 V. Organic cathodes were prepared by mixing PAQS/CNTs composite with Printex XE2 carbon black and PTFE binder in a 60:30:10 weight ratio. All the components and some isopropanol were added into a ball mill jar and homogenized for 30 min on Retsch PM100 at 300 rpm. Composite was then rolled in between a glass plate and a sheet of baking paper to give self-standing electrodes. Afterwards 12 mm self-standing electrodes were cut, dried and transferred into the glovebox. The loading of active material was around 2 mg cm^{-2}. Cells for *ex situ* measurements were assembled with two layers of glassy fiber separator and one additional layer of Celgard separator on the cathode side to prevent entanglement of fibers from the separator on the cathode and simplify the removal of cathodes from cells. To improve the mechanical stability of electrodes for *ex situ* characterization, electrodes were pressed on Al foil current collector with 2 t cm^{-2}. Mg foil (0.1 mm, 99.95%, Changsha Rich Nonferrous metals) was polished with P1200 sandpaper inside the glovebox shortly before assembly and used as an anode. Electrochemical testing of the cathodes was performed under galvanostatic mode with VMP3 potentiostat from Bio Logic S. A. in Swagelok type cells.

Ex situ electrode characterization

IR characterization was performed inside the glovebox using ATR-IR Alpha II (Bruker) equipped with Ge crystal. Measurements were performed in the range from 4000 to 600 cm^{-1}. Cathodes for *ex situ* measurements were charged or discharged with 0.5 C rate. Afterwards, cathodes were disassembled inside the glove box, washed 2 times with a 2 mL of DME to remove residual electrolyte and dried before IR spectra were measured. Scanning electron microscopy (SEM) was performed with a field emission Supra 35 VP Carl Zeiss microscope coupled with the energy dispersive spectrometer (EDS) at 20 kV of accelerating voltage. Samples were prepared inside the glovebox and transferred into the SEM by a home-made vacuum sample transfer chamber to avoid contamination by either moisture or air.

2. Results and Discussion

At the beginning of this work, electrochemical performance of two magnesium fluorinatedalkoxyborate electrolytes was compared. Both MgBhfip and MgFPB salts were synthesized according to the literature[19,20] through deprotonation of fluorinated alcohol with BH_4^-. After isolation, salts were characterized using NMR and IR spectroscopy to check that deprotonation of $Mg(BH_4)_2$ was complete. IR spectra of MgFPB and MgBhfip salts confirmed the complete conversion of $Mg(BH_4)_2$, since characteristic peak for B–H stretching at 2274 cm^{-1} could not be detected (Figure S1, S2). In the spectrum of MgFPB (Figure 1a) we can identify strong peaks at 1227 and 1203 cm^{-1}, which are attributed to the B–O–C stretching vibrations and $-CF_3$ symmetric and antisymmetric stretching vibrations. Additionally, due to the deformation mode of $-CF_3$ group, a medium intensity peak at 865 cm^{-1} can be observed. Peaks at 1071, 1043 and 1010 cm^{-1} correspond to C–O stretching vibrations due to DME molecules coordinated to Mg cation, which display also C–H deformation of methyl and methylene groups as a low intensity broad peak at 1471 cm^{-1}. MgFPB does not have any protons; therefore, ^1H NMR spectrum shows only protons from DME molecules (Figure S3). The absence of –OH peak at 9.51 in ^1H NMR again confirms that the surplus of alcohol was successfully removed during isolation. ^{19}F spectrum of the salt shows one peak at −70.36 ppm for 48 equivalent F atoms (Figure 1b), which is in the agreement with the literature.[20] Due to the similar structure of prepared salts, IR spectrum of MgBhfip is similar to the one of MgFPB. Characteristic bands for C–H, C–CF_3, B–O–C, C–O stretching and CF_3 deformation modes were observed. A specific difference is the peak of C–H stretching from $Bhfip^-$ anion at 2953 cm^{-1} (Figure S2). Besides protons from DME molecules, ^1H NMR spectrum of MgBhfip salt shows a peak at 4.43 ppm, which is attributed to 8 protons from hfip ligands (Figure S4). Characterization is consistent with the literature.[15]

Mg deposition/stripping performance of MgFPB and MgBhfip was compared in DGM based electrolytes (Figure S5). MgBhfip exemplified lower starting overpotential and higher Coulombic efficiency in the starting cycles, but the efficiency of MgBhfip started to gradually decrease already from the 1st cycle and dropped to 91% in the 20th cycle. Similarly, overpotential also started to increase after the first 10 cycles. On the other hand, the overpotential of MgFPB decreased in initial cycles and stabilized, while the Coulombic efficiency increased and stabilized around 96%. These results are in good agreement with the literature report,[20] which lead us to choose MgFPB for further optimization. As a next step MgFPB was tested in the DME solvent, which is a more commonly used solvent for Mg electrolytes, especially in the testing of Mg metal–organic battery system.[5,19,30] However, electrolyte in DGM exhibited better performance than in DME both in terms of Coulombic efficiency and overpotential (Figure S6). Coulombic efficiency in DGM electrolyte stabilizes after a few initial cycles, while in DME electrolyte it varied quite a lot through all 20 cycles. Furthermore, after approximately 10 cycles potential instabilities are observed, which also substantially contribute to the scatter of Coulombic efficiency. Comparison of overpotentials reveals that DGM electrolyte exhibits lower values (difference of around 80 mV) than its DME analogue, which contributes to improved energy efficiency of the Mg metal anode battery with DGM based electrolyte.

Although Coulombic efficiency of 96% is promising for a chloride-free electrolyte and might have been even considered revolutionary just a few years ago, it still falls short of the targeted efficiency for practical cell applications. Different electrolyte impurities like water can tremendously affect Mg stripping/deposition process.[31] The addition of Bu_2Mg (di-*n*-butyl magnesium), which acts like a scavenger can help to improve the electrochemical performance of the electrolyte both in terms of the overpotential and Coulombic efficiency.[32] Thus, 40 mM of Bu_2Mg was added to DME and DGM based MgFPB electrolytes. Their Coulombic efficiency is compared in Figure 2. The electrolyte in DME, similar to the one without the addition of Bu_2Mg, shows unstable behavior. In the first 10 cycles Coulombic efficiency increases to 99%, followed by a fade to around 96%. In the case where MgFPB/Bu_2Mg salts are dissolved in DGM, Coulombic efficiency in the first cycle is just below 85% but after 5 cycles it increases up to 97% where it stabilizes. Again, a cell with DGM electrolyte displays lower

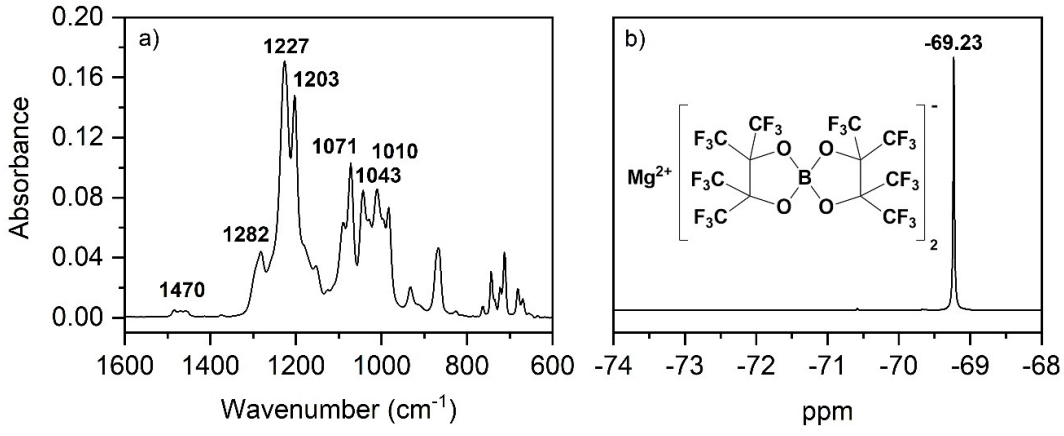

Figure 1. a) IR and b) ^{19}F NMR spectra of MgFPB with the structure of the salt.

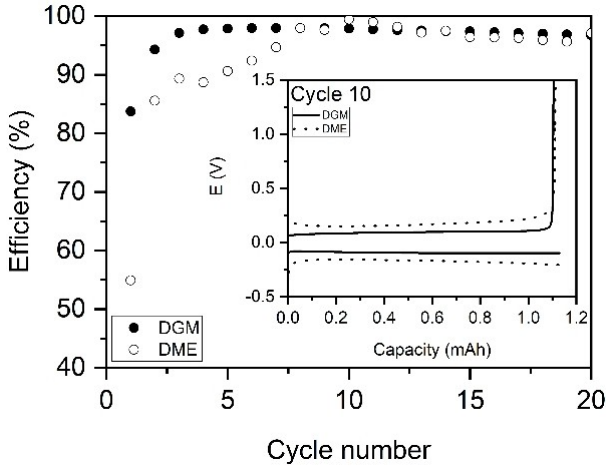

Figure 2. Comparison of Coulombic efficiency of MgFPB/*n*-Bu_2Mg electrolyte in DGM (solid dot) and in DME (empty dot) on Pt at 1 mA cm^{-2}. Inset: comparison of overpotentials in the 10th cycle of Mg stripping and deposition.

overpotentials than the one with DME electrolyte. After 20 cycles overpotential stabilizes at 140 mV for DME and at 80 mV for DGM electrolyte. Therefore, by comparing the electrochemical performance of MgFPB and MgFPB/Bu_2Mg electrolyte in the same solvent, we observe a decrease of polarization for about 20 mV in DGM and 30 mV in DME when Bu_2Mg is added.

It should be noted that in Mg stripping/deposition tests using electrolytes based on MgFPB and MgBhfip salts exhibit certain instability above 2 V during stripping (Figure S7). In the literature, such behavior has not yet been reported, but the stripping of Mg metal is typically done only up to 0.8 V, which effectively avoids the problematic potential area.[19] Comparing electrolytes with and without Bu_2Mg, this phenomenon starts approximately 20 cycles later, when Bu_2Mg is added. Hence, we hypothesize that instabilities could be explained by partial passivation of the working electrode and consequentially more localized Mg deposition. Localized Mg deposition can lead to micro short circuits, which can be only transient in their nature due to on-going Mg stripping/deposition. Localized Mg deposition can be successfully mitigated through the use of the conductive carbon interlayer, which increases Mg metal stripping/deposition efficiency and decreases its overpotential.[33]

Good electrochemical Mg stripping/deposition of MgFPB/Bu_2Mg/DGM electrolyte opened the possibility for testing of the organic cathode material. First cathode tests were performed using plain PAQS polymer, which has already been tested extensively in chloride based Mg electrolytes.[26,34] However, in the initial test only 40% of theoretical capacity was obtained (90 mAh g^{-1}) (Figure S8). Low capacity utilization is often connected with improper electrochemical wiring of active material in the composite electrode, and with it connected sluggish transport. Thus, we decided to utilize PAQS polymer composite, which was prepared by *in situ* polymerization in the suspension of CNTs. Role of CNTs nanostructurization was to improve the electronic and ionic wiring of the electrode composite. PAQS/CNTs composite (Figure 3) displays significantly better capacity utilization, with a first discharge capacity of 171 mAh g^{-1} (76% of the theoretical capacity). Initial high discharge capacity is followed by gradual capacity fade down to 148 mAh g^{-1} in 20th cycle. Afterwards, capacity fade is accelerated and in the 100th cycle only 64 mAh g^{-1} of capacity is retained. Coulombic efficiency in initial cycles is high, around 99%, followed by a decrease for 8% through first 50 cycles. After that, the efficiency is slowly increasing, reaching 93% in the 100th cycle. The discharge electrochemical plateau is observed at 1.58 V in the first 20 cycles, but it gradually degrades during cycling, pointing to the gradual, but continuous dissolution of active material, which was already observed in previous test with chloride based electrolytes.[26] PAQS polymer is mostly synthesized in form of oligomers, which is evident from the relatively low ratio between linker/end groups (S/Cl) (Table 1, below).

Mg metal–PAQS/CNTs cells were also tested at elevated current densities, which are important for practical application, especially if we are targeting electromobility and stationary storage applications, where power densities are highly impor-

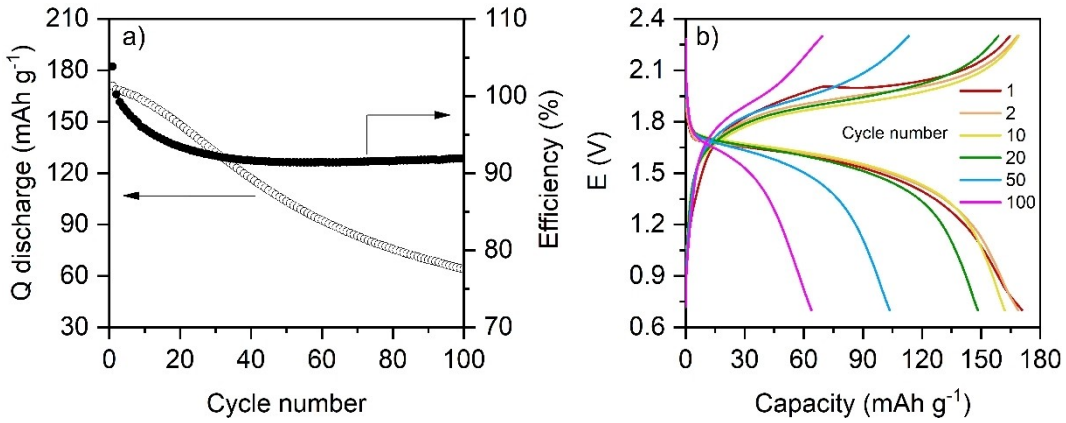

Figure 3. a) Discharge capacity and Coulombic efficiency of Mg metal–PAQS/CNTs battery at 0.5 C in the voltage window from 0.7 to 2.3 V. b) Selected discharge/charge profiles.

tant. Rate capability tests were performed in the range from 0.5 C to 20 C. Capacity drop at intermediate rates of 1 C (84%) and 2 C (71%) indicates some kinetic limitations, the drop is more significant at 5 C (52%) and 10 C (31%) (Figure 4). At the highest rate capability of 20 C only slightly more than 10% of the capacity is retained and we can clearly observe almost complete loss of the electrochemical plateau (Figure 4b), meaning that most of the capacity originates from the capacitance. Given, the relatively low overpotential for Mg stripping/deposition at 1 mA/cm^2 and good performance of the polymer in Li battery system (Figure S9), transport limitations are most likely connected with the migration of Mg species within the organic cathode. The capacity retention at high current densities still has some room for improvement either by electrolyte modification or further structuration of cathode composite.

The anthraquinone electrochemical group belongs to conjugated carbonyl compounds, which are n-type electrode materials and undergo the reduction of conjugated carbonyl bond to phenoxylate salt during electrochemical discharge. Their electrochemical mechanism can be effectively studied through *operando* and *ex situ* ATR-IR spectroscopy.[34–36] Therefore, *ex situ* PAQS/CNTs electrodes at different states of the charge were prepared (Figure S10) and studied with ATR-IR spectroscopy (Figure 5 and S11). Upon discharge the relative intensity of the carbonyl peaks at 1673 and 1650 cm^{-1} decreased, but peaks still remained visible, consistent with the incomplete capacity utilization. At the same time, a new, well defined peak at 1379 cm^{-1} appears. This peak is consistent with

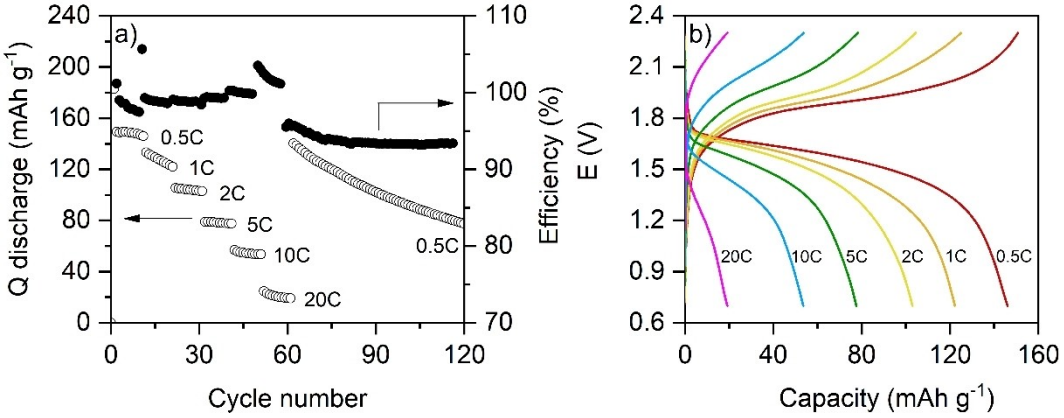

Figure 4. a) Rate capability and CE of PAQS/CNTs in the Mg/PAQS/CNTs battery with MgFPB/Bu_2Mg/DGM electrolyte at 0.5–20 C current densities; b) Selected different C-rates charge/discharge galvanostatic curves; cut of voltage 0.7–2.3 V.

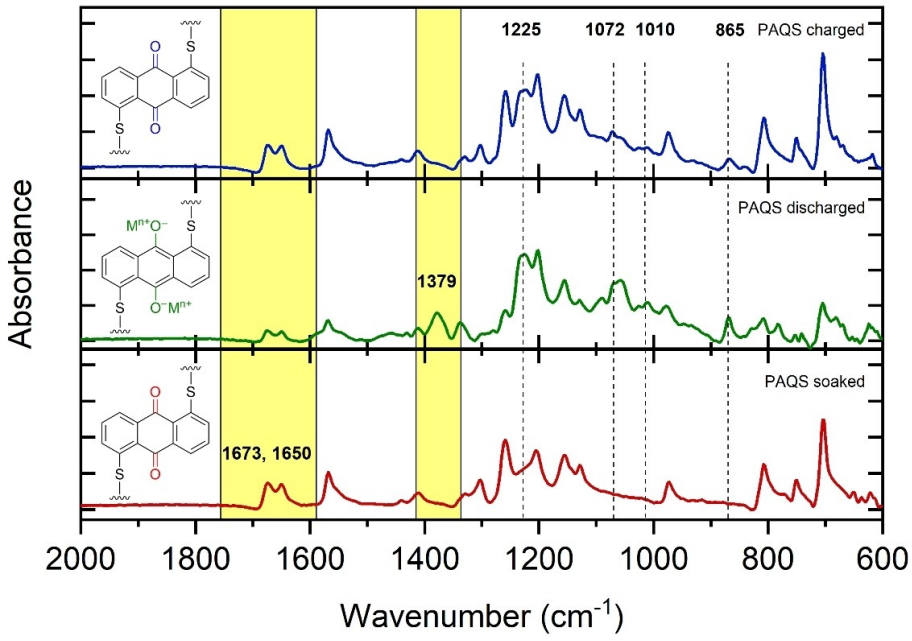

Figure 5. IR spectra of the PAQS/CNTs *ex situ* electrodes. On the left side: schematic of the mechanism during charge and discharge of PAQS/MgFPB/Mg battery.

the formation of the phenoxylate group.[36] There are several new peaks in the discharged cathode that can be connected with the presence of FPB anion in the electrode. These are peaks at 1225 and 1072 (C–B, CF_3), 1010 (C–O) and 865 cm^{-1} (CF_3). Upon charge, the intensity of carbonyl peak increases and phenoxylate peak almost completely disappears. However, the remainder of peaks related to the FPB anion is still present pointing to either incomplete recharge or some chemical degradation of the salt on the surface of the polymer. ATR-IR characterization of cycled electrodes composed of only conductive carbon and binder (Figure S12) shows the absence of electrolyte peaks pointing to the fact that degradation of salt does not occur on conductive carbon or binder. Therefore, incomplete charging is the most likely reason for the presence of FPB peaks in the spectrum of the charged PAQS/CNTs electrode, although degradation of electrolyte on the polymer surface cannot be excluded.

The presence of anions in the discharged cathode suggests that cations compensating the negative charge on discharged anthraquinone groups are not exclusively Mg^{2+} cations but at least partially $MgFPB^+$ monovalent cations. In the case of Mg batteries, this has already been observed for chloride electrolytes, but it was shown that it can vary strongly between different Mg electrolytes.[27,35] The inclusion of salt anions in the overall electrochemical reaction greatly limits the achievable energy density of the battery cell due to the need for large amount of salt in the cell and prevents operation in the conditions of the lean electrolyte. EDS characterization of *ex situ* electrodes (Table 2) demonstrates that the amount of F in the discharged electrode increases significantly during discharge and then decreases during charge. No Mg signal in the soaked electrode means that our washing procedure was effective, and we were able to fully wash away the salt that was not involved in the electrochemical reaction. Subtracting the amount of F that was detected in the pristine electrode due to polytetrafluoroethylene (PTFE) binder, allowed us to determine the amount of active F connected with FPB anion (Details about the calculation are available in SI). If we divide this increase of F with 24 F atoms per FPB anion, we get the ratio of 4:1 between Mg^{2+} and $MgFPB^+$ species. This is supported by the fact that the mass increase of discharged cathode is 40%. If all of the negative charge in our electrode (given the capacity obtained in discharge of *ex situ* electrode) would be compensated by Mg^{2+} we would expect a mass increase of only 3%. Contrary, coordination of reduced carbonyl exclusively with monovalent $MgFPB^+$ cation would lead to a mass increase of 155%. Obtained ratio 4:1 between bare Mg^{2+} and $MgFPB^+$ coordination is much better to the ones previously obtained in chloride based electrolytes, where values ranging from 1.5:1 between Mg^{2+}:$MgCl^+$ to exclusive $MgCl^+$ coordination were reported.[27,35] This gives promise for future high-energy Mg metal-organic batteries, in which sole Mg^{2+} coordination would enable operation in lean electrolyte conditions.

While the electrochemical mechanism of PAQS/CNT was successfully confirmed, the long-term capacity is far from satisfactory. This lead us to test another polymer, PFQ/rGO, which exhibited much better capacity retention already in chloride based electrolytes.[37] Indeed, much better capacity retention than in the case of PAQS/CNTs was observed. A maximum capacity of 122 mAh g^{-1} was obtained after approximately 40 cycles. After 250 cycles 85 mAh/g was still retained, demonstrating 69% capacity retention (Figure S13), which points to the fact that good long-term performance can be achieved by synthesis of suitable polymer material. However, capacity utilization of PFQ/rGO (compared with PAQS/CNT material) was lower, which means there remains a significant challenge of material development that would combine both long-term capacity retention and good capacity utilization.

3. Conclusions

In this work, we have investigated electrochemical compatibility of organic cathode based on anthraquinone and phenanthraquionone polymers with fluorinated alkoxyborate electrolyte. It was shown that electrochemical performance can be improved by use of suitable solvent and additives. Initial electrochemical characterization with PAQS organic cathode showed limited capacity, only around 40% of the theoretical. After nanostructurization, polymer capacity utilization increased to 76%, but long-term capacity still remained unsatisfactory. Significant improvement of the long-term cycling performance was achieved by using long-chain phenanthrenequinone polymer, demonstrating the need for a new generation of cathode materials which should at the same time exemplify high capacity utilization and long-term capacity retention. Investigation of the electrochemical mechanism of anthraquinone polymer through *ex situ* ATR-IR confirmed reduction of carbonyl group during discharge, consistent with the electrochemical mechanism in chloride based electrolytes. Even though fluorinated alkoxyborate class of Mg salts should enable more facile dissociation of Mg^{2+} cation we were still able to identify salt anions and with it non-dissociated $MgFPB^+$ in the discharged cathode. The extent of monovalent cations pres-

Table 2. SEM EDS analysis of *ex situ* PAQS/CNTs electrodes. Atomic ratios are normalized per S content, which is presumed to remain constant during charge/discharge. All the spectra were measured at least on 4 sites and average values are presented.

Electrode	C	O	F	F active	S	Cl[a]	Mg	Mass increase
Pristine (soaked)	33	2.4	3.4	0.00	1.0	0.17	0.00	/
Discharged	35	4.1	6.3	2.9	1.0	0.17	0.60	40%
Charged	33	2.6	4.6	1.2	1.0	0.15	0.13	13%

[a] Please note that a small amount of chlorine in electrodes comes from the PAQS polymer, which is synthesized from 1,5-dichloroanthraquinone monomer and some chlorine atoms remain in the final polymer as end groups.

ence was significantly lower than in chloride based electrolytes, where, in certain cases, exclusive $MgCl^+$ coordination was observed. This fact holds promise for the future development of Mg-organic batteries in lean electrolyte conditions, a prerequisite requirement for realization of practical high-energy density Mg metal−organic battery.

Acknowledgements

The authors would like to acknowledge financial support from Slovenian Research Agency under research projects Z2-1864 and J2-8167 and research programme P2-0393 and Honda R&D Germany. T.P. would like to acknowledge the Slovenian Research Agency for funding her Ph.D. work within Young Researchers framework.

Conflict of Interest

The authors declare no conflict of interest.

Keywords: chloride-free electrolytes · *ex situ* measurements · magnesium rechargeable batteries · organic materials · quinone-based polymers

[1] Communication on the 2017 list of Critical Raw Materials for the EU, http://eur-lex.europa.eu/legalcontent/EN/TXT/PDF/?uri=CELEX:52017DC0490&from=EN.
[2] M. Matsui, *J. Power Sources* **2011**, *196*, 7048–7055.
[3] M. Jäckle, K. Helmbrecht, M. Smits, D. Stottmeister, A. Groß, *Energy Environ. Sci.* **2018**, *11*, 3400–3407.
[4] M. S. Ding, T. Diemant, R. J. Behm, S. Passerini, G. A. Giffin, *J. Electrochem. Soc.* **2018**, *165*, 1983–1990.
[5] J. Bitenc, K. Pirnat, E. Žagar, A. Randon-Vitanova, R. Dominko, *J. Power Sources* **2019**, *430*, 90–94.
[6] A. Kopač Lautar, J. Bitenc, T. Rejec, R. Dominko, J.-S. Filhol, M.-L. Doublet, *J. Am. Chem. Soc.* **2020**, *142*, 5146–5153.
[7] R. Attias, M. Salama, B. Hirsch, Y. Goffer, D. Aurbach, *Joule* **2019**, *3*, 27–52.
[8] L. W. Gaddum, H. E. French, *J. Am. Chem. Soc.* **1927**, *49*, 1295–1299.
[9] J. H. Connor, W. E. Reid, G. B. Wood, *J. Electrochem. Soc.* **1957**, *104*, 38.
[10] A. Brenner, *J. Electrochem. Soc.* **1971**, *118*, 99.
[11] T. D. Gregory, *J. Electrochem. Soc.* **1990**, *137*, 775.
[12] D. Aurbach, Z. Lu, A. Schechter, Y. Gofer, H. Gizbar, R. Turgeman, Y. Cohen, M. Moshkovich, E. Levi, *Nature* **2000**, *407*, 724–727.
[13] R. E. Doe, R. Han, J. Hwang, A. J. Gmitter, I. Shterenberg, H. D. Yoo, N. Pour, D. Aurbach, *Chem. Commun.* **2014**, *50*, 243–245.
[14] S. He, K. V. Nielson, J. Luo, T. L. Liu, *Energy Storage Mater.* **2017**, *8*, 184–188.
[15] K. A. See, K. W. Chapman, L. Zhu, K. M. Wiaderek, O. J. Borkiewicz, C. J. Barile, P. J. Chupas, A. A. Gewirth, *J. Am. Chem. Soc.* **2016**, *138*, 328–337.
[16] J. Muldoon, C. B. Bucur, A. G. Oliver, J. Zajicek, G. D. Allred, W. C. Boggess, *Energy Environ. Sci.* **2013**, *6*, 482.
[17] R. Mohtadi, M. Matsui, T. S. Arthur, S. J. Hwang, *Angew. Chem. Int. Ed.* **2012**, *51*, 9780–9783; *Angew. Chem.* **2012**, *124*, 9918–9921.
[18] O. Tutusaus, R. Mohtadi, T. S. Arthur, F. Mizuno, E. G. Nelson, Y. V. Sevryugina, *Angew. Chem. Int. Ed.* **2015**, *54*, 7900–7904; *Angew. Chem.* **2015**, *127*, 8011–8015.
[19] Z. Zhao-Karger, M. E. Gil Bardaji, O. Fuhr, M. Fichtner, *J. Mater. Chem. A* **2017**, *5*, 10815–10820.
[20] J. Luo, Y. Bi, L. Zhang, X. Zhang, T. L. Liu, *Angew. Chem. Int. Ed.* **2019**, *58*, 6967–6971.
[21] J. T. Herb, C. A. Nist-Lund, C. B. Arnold, *ACS Energy Lett.* **2016**, *1*, 1227–1232.
[22] X. Sun, P. Bonnick, V. Duffort, M. Liu, G. Ceder, L. F. Nazar, *Energy Environ. Sci.* **2016**, *9*, 2273–2277.
[23] G. Gershinsky, H. D. Yoo, Y. Gofer, D. Aurbach, *Langmuir* **2013**, *29*, 10964–10972.
[24] R. Zhang, X. Yu, K.-W. Nam, C. Ling, T. S. Arthur, W. Song, A. M. Knapp, S. N. Ehrlich, X.-Q. Yang, M. Matsui, *Electrochem. Commun.* **2012**, *23*, 110–113.
[25] H. Sano, H. Senoh, M. Yao, H. Sakaebe, T. Kiyobayashi, *Chem. Lett.* **2012**, *41*, 1594–1596.
[26] J. Bitenc, K. Pirnat, T. Bančič, M. Gaberšček, B. Genorio, A. Randon-Vitanova, R. Dominko, *ChemSusChem* **2015**, *8*, 4128–4132.
[27] H. Dong, Y. Liang, H. Dong, Y. Liang, O. Tutusaus, R. Mohtadi, Y. Zhang, F. Hao, Y. Yao, *Joule* **2019**, 1–12.
[28] J. Bitenc, N. Lindahl, A. Vizintin, M. E. Abdelhamid, R. Dominko, P. Johansson, *Energy Storage Mater.* **2020**, *24*, 379–383.
[29] K. Pirnat, J. Bitenc, A. Vizintin, A. Krajnc, E. Tchernychova, *Chem. Mater.* **2018**, *30*, 5726–5732.
[30] I. Shterenberg, M. Salama, H. D. Yoo, Y. Gofer, J.-B. Park, Y.-K. Sun, D. Aurbach, *J. Electrochem. Soc.* **2015**, *162*, A7118–A7128.
[31] S. He, J. Luo, T. L. Liu, *J. Mater. Chem. A* **2017**, *5*, 12718–12722.
[32] I. Shterenberg, M. Salama, H. D. Yoo, Y. Gofer, J.-B. Park, Y.-K. Sun, D. Aurbach, *J. Electrochem. Soc.* **2015**, *162*, A7118–A7128.
[33] H.-D. Lim, D. H. Kim, S. Park, M. E. Lee, H.-J. Jin, S. Yu, S. H. Oh, Y. S. Yun, *ACS Appl. Mater. Interfaces* **2019**, *11*, 38754–38761.
[34] A. Vizintin, J. Bitenc, A. Kopač Lautar, K. Pirnat, J. Grdadolnik, J. Stare, A. Randon-Vitanova, R. Dominko, *Nat. Commun.* **2018**, *9*, 661.
[35] J. Bitenc, A. Vizintin, J. Grdadolnik, R. Dominko, *Energy Storage Mater.* **2019**, *21*, 347–353.
[36] J. Bitenc, T. Pavčnik, U. Košir, K. Pirnat, *Materials.* **2020**, *13*, 506.
[37] A. Vizintin, J. Bitenc, A. Kopač Lautar, J. Grdadolnik, A. Randon Vitanova, K. Pirnat, *ChemSusChem* **2020**, *13*, 2328–2336.

Manuscript received: November 30, 2020
Revised manuscript received: January 9, 2021
Accepted manuscript online: January 11, 2021
Version of record online: February 1, 2021